2011 50th IEEE Conference on Decision and Control and
European Control Conference (CDC-ECC)
Orlando, FL, USA, December 12-15, 2011

Design and Implementation of a Surge Controller for an AMB Supported Compressor in the Presence of Piping Acoustics

Se Young Yoon[†], Zongli Lin[†] and Paul E. Allaire[‡]

Abstract— **Active control of compressor surge using the thrust Active Magnetic Bearing (AMB) for unshrouded centrifugal compressors is revisited here. Based on a recently presented enhanced compression system model with variable impeller tip clearance and pipeline acoustics, a surge controller is designed. This controller calculates the command clearance between the impeller and the static shroud to create the necessary pressure modulation in the system to suppress the surge instability. The commanded impeller clearance is later fed to the thrust AMB to actuate the axial position of the compressor rotor. The proposed surge control method is derived and implemented on an experimental compressor setup, and test results for the surge controller are presented in this paper. Observations from the experimental surge testing demonstrate that the presented method is able to stabilize the compression system when operating in the unstable surge region, extending the stable flow range by over 21%. Also the derived controller shows good robustness to the internal AMB dynamics.**

I. Introduction

Surge is one of the main dynamics instability limiting the operation of centrifugal compressors. When a downstream load restricts the flow through the compression system beyond the stability limit, the pressure is built at the compressor exhaust and in the plenum volume until it surpasses the pressure field that the compressor can generate [1]. This event initiates a limit cycle that affects the entire system, and can cause extensive structural damage to the machine due to the violent vibration and high thermal loads that generally accompany the instability [2].

The concept of active stabilization of surge was initially introduced by Epstein in [3]. Since then, different sensors and actuators have been investigated in the control of surge in compression systems. Simon *et al.* demonstrated in [4] that selecting an accessible actuator with proven controllability of the compressor's unstable modes and enough bandwidth to stabilize the flow dynamics during surge is not a simple task. Arnulfi *et al.* in [5] and de Jager in [2] presented reviews of published works on both passive and active surge control, and their respective selections of actuators. Actuators commonly reported in the literature are the close-coupled valves [6] and the throttle valves [7].

The use of Active Magnetic Bearing (AMB) for the control of compressor surge in single stage centrifugal machines was previously presented in [8] and [9]. The concept was originally introduced by Sanadgol in [10], and numerical simulations were presented to support the idea. Sanadgol proposed servo controlling the impeller axial displacement with the thrust AMB, effectively changing clearance between the impeller and the static shroud. This would induce a pressure variation that could be employed to stabilize surge. A preliminary mathematical model describing the compression system with AMBs was introduced in [10], and an enhancement to the model based on experimental measurements was presented by Yoon *et al.* in [11].

In this paper, we present new experimental results in the control of compressor surge using the AMBs in the compressor. For a centrifugal compressor test rig supported on AMBs that was commissioned for this study, and based on the enhanced compression system model that was recently presented in [11], a surge controller is designed, implemented and tested. The proposed controller relies on the accurate control of the impeller axial position by the AMB to maintain the compressor operation in a neighborhood of the equilibrium point. More specifically, the experimental setup will be introduced in Section II and the modeling of the compression system will be discussed in Section III. Section IV will present the derivation of the surge control law, whose effectiveness is guaranteed for a family of possible AMB closed-loop dynamics. Experimental surge control results will be presented in Section V, and conclusions in Section VI.

II. Experimental Setup

A compressor test rig was built and commissioned for the study of surge control with the use of AMBs. A photograph of the test rig, which was presented in details in [11] and [12], is shown in Fig. 1. A drawing showing the layout of the experimental setup is presented in Fig. 2. The experimental system consists of a single stage centrifugal compressor, a modular ducting system at the compressor inlet and exhaust, and a throttle valve controlling the flow rate through the system. The ducting system is designed so the throttle valve can be positioned at different predetermined locations along the exhaust piping, effectively modifying the plenum volume of the system. Additionally, steady state flow rate, static pressure and temperature sensors are installed along the inlet and exhaust piping to monitor the flow condition throughout the compression system.

The centrifugal compressor in the experimental setup is a single state machine with an unshrouded impeller. As shown in Fig. 3, the compressor rotor is supported by two radial AMBs at each end of the compressor, and a thrust AMB controlling the axial rotor displacement and the clearance

[†]S. Y. Yoon and Z. Lin are with Charles L., Brown Department of Electrical and Computer Engineering, University of Virginia, Charlottesville, VA 22904-4743, USA.

[‡]P. E. Allaire is with the Department of Mechanical and Aerospace Engineering, University of Virginia, Charlottesville, VA 22904-4746, USA.

978-1-61284-799-3/11/$26.00 ©2011 IEEE

Fig. 1. Photograph of the compressor test rig in inlet and exhaust piping.

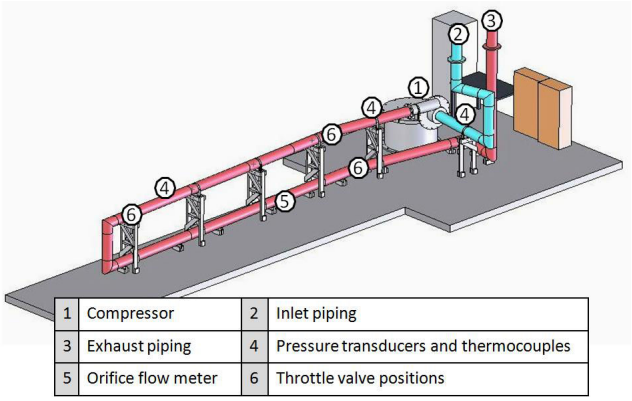

Fig. 2. The compressor test rig has a centrifugal compressor, instrumentations along the inlet and exhaust piping, and a throttle valve that can be located at 2.2 m, 7.1 m and 15.2 m down the exhaust piping measured from the compressor.

between the impeller and the static shroud. The AMBs are unstable systems, thus they require a feedback position loop to stabilize the rotor at the reference position. The maximum load capacity of the thrust bearing is 6,600 N, which is estimated to be sufficient to support the rotor during surge and to actuate the impeller position. A high speed electric motor coupled to the compressor shaft drives the system to a maximum speed of 17,000 rpm.

III. System Modeling

The dynamic model of the compression system considered here was presented in details in [11] and [13]. The equations describing the dynamics of the compression system is based on the well-known Greitzer model. The nondimensional pressure rise Ψ and mass flow rate Φ are defined as the following functions of the mass flow rate m and pressure P,

$$\Phi = \frac{m}{\rho_{o1} U A_c}, \quad \Psi = \frac{P - P_{o1}}{\frac{1}{2}\rho_{o1} U^2}. \tag{1}$$

The constants in Eq. (1) are the impeller tip velocity U, the cross section area of the compressor duct A_c, the inlet absolute pressure P_{o1}, and the density at the inlet ρ_{o1}.

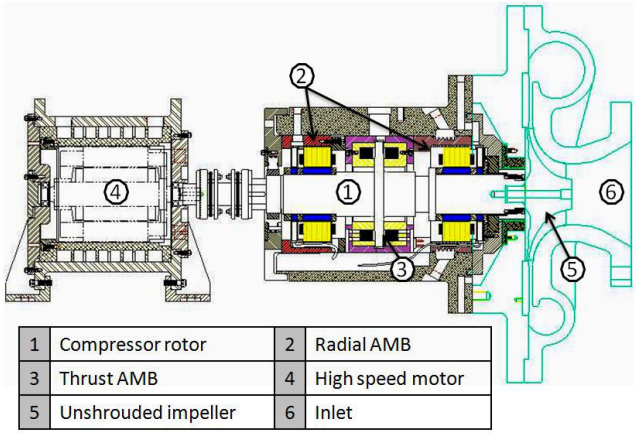

Fig. 3. Single state centrifugal compressor with unshrouded impeller and rotor supported on AMBs.

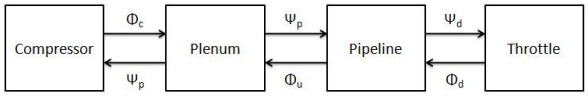

Fig. 4. Block diagram of the compression system model with pipeline dynamics.

The Greitzer model can capture the surge limit cycle for a compression system, and it serves as a good basis for development of surge control laws. As described in [11], the acoustic resonance from the compressor pipeline is added to the model. The resulting block diagram for the compression system with pipeline dynamics is shown in Fig. 4.

A. Compressor and Plenum

The basis of the equations describing the flow in the compressor and the plenum volume comes from the Greitzer model in [14]. This model assumes a low compressor inlet match number, low pressure rise compared to ambient pressure, plenum isentropic compression process with uniform distribution, and negligible fluid velocities in the plenum. The active magnetic bearings supporting the compressor spindle allow the impeller to move axially and change the horizontal clearance between the impeller tip and the static shroud δ_{cl}. This extra capability of the AMBs was added in the dynamics model in [9] and [10] by introducing a tip clearance constant k. The resulting system equations are

$$\dot{\Phi}_c = B\omega_H \left(\Psi_{c,ss}(\Phi_c) + \frac{P_{o1}}{\frac{1}{2}\rho_{o1} U^2} k\delta_{cl} - \Psi_p \right), \tag{2a}$$

$$\dot{\Psi}_p = \frac{\omega_H}{B} \left(\Phi_c - \Phi_p \right), \tag{2b}$$

where B is the Greitzer stability parameter, ω_H is the Helmholtz frequency, as defined in the original Greitzer model in [14]. The state variables of the model are the compressor mass flow rate Φ_c, and the plenum pressure rise Ψ_p, which are nondimensionalized as shown in Eq. (1). The value of the plenum mass flow rate Φ_p is dependant on the dynamics of the piping. Lastly, the steady state compressor

pressure rise $\Psi_{c,ss}$ is a function of the compressor mass flow, and it is defined as the point in the characteristic curve corresponding to the compressor mass flow rate,

$$\Psi_{c,ss}(\Phi_c) = A_1\Phi_c^3 + B_1\Phi_c^2 + D_1. \quad (3)$$

The polynomial coefficients A_1, B_1 and D_1 of the characteristic curve are obtained following the method in [15] for finding the third order polynomial fitting of the compressor measured characteristics.

The variation of the impeller tip clearance δ_{cl} enters the compressor equation in Eq. (2) as a proportional change in the compressor pressure rise. This is a linear approximation introduced in [10], where the constant k is defined as

$$k = -\frac{\gamma}{\gamma-1}\frac{0.7}{b+0.7cl_0}\psi_{c,ss}^{\frac{1}{\gamma}}\left(1-\psi_{c,ss}^{\frac{\gamma-1}{\gamma}}\right), \quad (4a)$$

$$\psi_{c,ss} = \left(\frac{\frac{1}{2}\rho U^2}{P_{o1}}\Psi_{c,ss}+1\right). \quad (4b)$$

Based on experimental observations, the above expression was corrected from [10] to match the response of the test rig. The other constants in the expression are the specific heat ratio γ, the design tip clearance cl_0, and the impeller tip blade height b. An analysis of the error introduced by the linearization of the tip clearance term is presented in [10], which verified the validity of the linearized approximation.

B. Piping

A modal approximation of the transmission line dynamics was presented in [16], and this model has been included in the compression system equations in [11] to describe the dynamics of the piping system. The single mode state space representation of the piping equations is given as

$$\begin{bmatrix}\dot{P}_{th}\\ \dot{Q}_p\end{bmatrix} = \begin{bmatrix}0 & -\frac{Z_0\pi}{2D_n}\\ \frac{\pi}{2D_nZ_0} & -8\end{bmatrix}\begin{bmatrix}P_{th}\\ Q_p\end{bmatrix} + \begin{bmatrix}0 & -\frac{2Z_0}{D_n}\\ \frac{2}{Z_0D_n} & 0\end{bmatrix}\begin{bmatrix}P_p\\ Q_{th}\end{bmatrix}, \quad (5)$$

where P_p and Q_p are the upstream (plenum) pressure and volumetric flow rate, respectively, as shown in Fig. 4. In the same way, P_{th} and Q_{th} are the downstream (throttle) pressure and flow rate. Other parameters in the model are the line impedance constant Z_0 and the line dissipation number D_n as defined in [16]. A steady state correction is added in the model as described in [16], and the resulting state space system has the structure of

$$\begin{bmatrix}\dot{P}_{th}\\ \dot{Q}_p\end{bmatrix} = \begin{bmatrix}0 & A_{12}\\ A_{21} & A_{22}\end{bmatrix}\begin{bmatrix}P_{th}\\ Q_p\end{bmatrix} + \begin{bmatrix}0 & B_{12}\\ B_{21} & 0\end{bmatrix}\begin{bmatrix}P_p\\ Q_{th}\end{bmatrix}, \quad (6)$$

The above piping model represents the system in terms of the pressure and volumetric flow rate. Assuming that the change of density of the gas in the pipeline ρ due the pressure and temperature fluctuation caused by the piping acoustics is small, the states of the piping model can be nondimensionalized as given in Eq. (1) as

$$\begin{bmatrix}\dot{\Psi}_{th}\\ \dot{\Phi}_p\end{bmatrix} = \begin{bmatrix}0 & \frac{2A_{12}A_c}{\rho U}\\ \frac{A_{21}\rho U}{2A_c} & A_{22}\end{bmatrix}\begin{bmatrix}\Psi_{th}\\ \Phi_p\end{bmatrix} + \begin{bmatrix}0 & \frac{2B_{12}A_c}{\rho U}\\ \frac{B_{21}\rho U}{2A_c} & 0\end{bmatrix}\begin{bmatrix}\Psi_p\\ \Phi_{th}\end{bmatrix} + \begin{bmatrix}0\\ \frac{\rho P_{o1}}{\rho_{o1}UA_c}(A_{21}+B_{21})\end{bmatrix}. \quad (7)$$

C. Throttle Valve

The flow rate through the throttle valve is a function of the pressure drop across the valve. Here, we assume that the dynamics at the throttle duct section are much faster than the rest of the system, and only the steady state behavior is captured. The relationship between the pressure and the mass flow rate in the throttle valve section is given by

$$\Phi_{th} = c_{th}u_{th}\sqrt{\Psi_{th}}, \quad (8)$$

where c_{th} is the valve constant and u_{th} is the throttle valve opening percentage.

D. Total Assembly

The completed system in Fig. 4 is obtained by combining Eqs. (2), (7) and (8). The resulting nonlinear system has the compressor mass flow, the plenum pressure rise, the throttle section pressure rise and the plenum mass flow rate as state variables,

$$\dot{\Phi}_c = B\omega_H\left(A_1\Phi_c^3+B_1\Phi_c^2+D_1+\frac{P_{o1}}{\frac{1}{2}\rho U^2}k\delta_{cl}-\Psi_p\right), \quad (9a)$$

$$\dot{\Psi}_p = \frac{\omega_H}{B}(\Phi_c-\Phi_p), \quad (9b)$$

$$\dot{\Psi}_{th} = \frac{2A_{12}A_c}{\rho U}\Phi_p + \frac{2B_{12}A_c}{\rho U}u_{th}c_{th}\sqrt{\Psi_{th}}, \quad (9c)$$

$$\dot{\Phi}_p = \frac{A_{21}\rho U}{2A_c}\Psi_{th} + A_{22}\Phi_p + B_{22}u_{th}c_{th}\sqrt{\Psi_{th}} + \frac{B_{21}\rho U}{2A_c}\Psi_p + \frac{\rho P_{o1}}{\rho_{o1}UA_c}(A_{21}+B_{21}). \quad (9d)$$

The parameters of the theoretical model are summarized in Table I. The coefficients of the characteristic curve given in this table corresponds to the corrected value for the unstable operating region of the compressor as described in [8]. The response of the assembled equations was compared to experimental measurements in [11] and [13] to validate the derived model. The Bode plots from the tip clearance to the plenum pressure is presented in Fig. 5 at 16,290 rpm and 20% throttle valve opening. We observe from this test a good agreement between the model and the experimental system, in both the magnitude and the phase responses. Two resonances are observed in the magnitude plot corresponding to the Helmholtz frequency and the piping acoustic resonance.

E. System Linearization

The compression system dynamics are linearized at the equilibrium operating point (Ψ_{eq}, Φ_{eq}), given by the intersection of the load curve corresponding to a selected throttle valve opening value of $u_{th,eq} = 0.17$ and the compressor characteristic curve. Define the new states of the compression system ξ_i to be the variation of the original i^{th} state variable of the system from the corresponding equilibrium value,

$$\xi_1 = \Phi_c - \Phi_{eq}, \quad (10a)$$

$$\xi_2 = \Psi_p - \Psi_{eq}, \quad (10b)$$

$$\xi_3 = \Psi_{th} - \Psi_{eq}, \quad (10c)$$

$$\xi_4 = \Phi_p - \Phi_{eq}. \quad (10d)$$

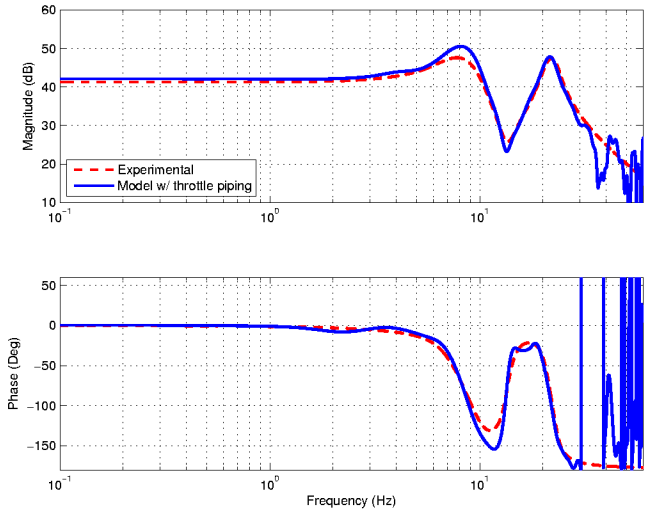

Fig. 5. Comparison of the theoretical and experimental Bode plots from the variation of the impeller tip clearance δ_{cl} to the nondimensional plenum pressure rise Ψ_{p} at 16,290 rpm and 20% throttle valve opening.

TABLE I
MODEL PARAMETERS FOR THE EXPERIMENTAL COMPRESSION SYSTEM

Parameter	Symbol	Unit	Value
Comp. duct length	L_{c}	m	1.86
Comp. duct cross. area	A_{c}	m^2	0.0082
Corrected A_1 coeff.	A_1	–	-13.23
Corrected B_1 coeff.	B_1	–	3.1479
Corrected D_1 coeff.	C_1	–	1.3007
Design tip clearance	cl_0	mm	0.6
Greitzer stab. parameter	B	–	0.44
Helmholtz freq.	ω_{H}	rad/s	80.1
Impeller tip speed	U	m/s	213.24
Impeller blade height	b	mm	8.21
Inlet pressure	P_{o1}	Pa	101,325
Inlet gas density	ρ_{o1}	Kg/m^3	1.165
Line dissipation number	D_{n}	–	2.83×10^{-5}
Line impedance constant	Z_0	Pa s/m	4.39×10^4
Plenum volume	V_{p}	m^3	0.049
Pipeline length	L	m	6.5
Throttle constant	c_{th}	–	1.8569

Using Taylor expansion we can approximate the system in Eq. (9) around the equilibrium operating point to be expressed in terms of the states defined in Eq. (10) as the state space system,

$$\begin{bmatrix} \dot{\xi}_1 \\ \dot{\xi}_2 \\ \dot{\xi}_3 \\ \dot{\xi}_4 \end{bmatrix} = \mathbf{A} \begin{bmatrix} \xi_1 \\ \xi_2 \\ \xi_3 \\ \xi_4 \end{bmatrix} + \begin{bmatrix} 2\frac{B\omega_{\text{H}} P_{\text{o1}} k}{\rho_{\text{o1}} U^2} \\ 0 \\ 0 \\ 0 \end{bmatrix} \delta_{\text{cl}}. \qquad (11)$$

The state matrix $\mathbf{A}$ of the above system is found to be

$$\mathbf{A} = \begin{bmatrix} \mathbf{a}_{11} & -B\omega_{\text{H}} & 0 & 0 \\ \frac{\omega_{\text{H}}}{B} & 0 & 0 & -\frac{\omega_{\text{H}}}{B} \\ 0 & 0 & \frac{B_{12} A_{\text{c}} u_{\text{th,eq}} c_{\text{th}}}{\rho U \sqrt{\Psi_{\text{eq}}}} & \frac{2A_{12}A_{\text{c}}}{\rho U} \\ 0 & \frac{B_{21}\rho U}{2A_{\text{c}}} & \frac{A_{21}\rho U}{2A_{\text{c}}} + \frac{B_{22} u_{\text{th}} c_{\text{th}}}{2\sqrt{\Psi_{\text{eq}}}} & A_{22} \end{bmatrix}, \qquad (12)$$

with $\mathbf{a}_{11} = B\omega_{\text{H}}(3A_1\Phi_{\text{eq}}^2 + 2B_1\Phi_{\text{eq}})$.

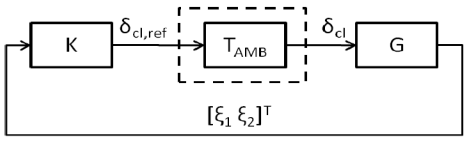

Fig. 6. Block diagram of the closed-loop compressor with surge control.

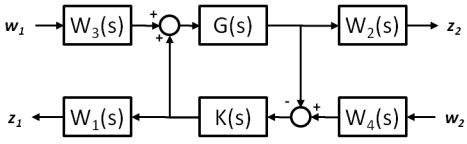

Fig. 7. Interconnected system for the synthesis of the H_∞ surge controller.

IV. SURGE CONTROLLER DERIVATION

In order to simplify the control problem, the stabilization of surge is decoupled from the control of the AMB system for rotor suspension. As shown in Fig. 6, the AMB controller forms an inner-loop regulating the rotor position, and the surge controller closes an outer loop to stabilize the compressor flow. The linearized compression system transfer function will be denoted as $G(s)$, the surge controller $K(s)$, and the internal closed-loop thrust AMB dynamics $T_{\text{amb}}(s)$. The input to the controller are the states ξ_1 and ξ_2, and the output is the reference tip clearance $\delta_{\text{cl,ref}}$.

A surge controller is designed from the linearized model in Eq. (11). As shown in Fig. 6, the surge controller computes the command signal for the impeller axial position from the compressor flow measurements, and the thrust AMB attempts to follow this reference impeller position. An error between the reference impeller clearance $\delta_{\text{cl,ref}}$ and the actual clearance δ_{cl} will be added during the actuation of the impeller position, which degrades the effectiveness of the surge controller. It was demonstrated in [8] and [9] that the surge controller $K(s)$ is stabilizing with the closed-loop AMB dynamics $T_{\text{amb}}(s)$ in the control loop if and only if it satisfies the inequality

$$\left| (I + KG)^{-1} KG \left(I - T_{\text{amb}} \right) \right|_\infty \leq 1. \qquad (13)$$

A controller satisfying the above inequality can be found using the H_∞ design scheme with the interconnected system shown in Fig. 7. The input-output transfer function matrix for the interconnected system is found to be

$$\begin{bmatrix} z_1 \\ z_2 \end{bmatrix} = \begin{bmatrix} -W_1 S_i K G W_3 & W_1 S_i K W_4 \\ W_2 S_o G W_3 & W_2 S_o G K W_4 \end{bmatrix} \begin{bmatrix} w_1 \\ w_2 \end{bmatrix}, \qquad (14)$$

where s was dropped to simplify the notation, and

$$S_i = (I + KG)^{-1}, \quad S_o = (I + GK)^{-1}.$$

The functions $W_i(s)$ for i from 1 to 4, are the weighting functions of the H_∞ scheme.

In the design of the surge controller, we approximate the dynamics T_{amb} from the reference $\delta_{\text{cl,ref}}$ to the actual δ_{cl} impeller tip clearance to be given by a 3rd order low-pass Butterworth filter with bandwidth of 70 Hz. An appropriate set of weighting functions for the selected AMB dynamics

T_{amb} are found to be

$$W_1(s) = I, \tag{15a}$$

$$W_2(s) = 0.001I, \tag{15b}$$

$$W_3(s) = \frac{2(s+0.1)}{s+300}I, \tag{15c}$$

$$W_4(s) = \frac{2000(s+0.1)}{s+3000}\begin{bmatrix} 1.5 & 0 \\ 0 & 1 \end{bmatrix}. \tag{15d}$$

The weighting function $W_3(s)$ was selected such that it bounds the magnitude of the sensitivity function as described in the stability condition in Eq. (13). On the other hand, $W_4(s)$ was selected to prioritize the pressure feedback signal for the computation of the control input, since this signal was found to be cleaner and more reliable that the flow rate. A sixth-order H_∞ controller is synthesized with the above weighting functions.

Transient mass flow measurements are not available in the experimental setup for feedback. A mass flow observer, that was derived in [9] following the results presented in [17], is expanded to include the piping dynamics. The state equation for the observer are given as

$$\dot{z} = B\omega_{\text{H}}\left(\hat{\Psi}_{\text{c,ss}} + \frac{P_{\text{o1}}}{\frac{1}{2}\rho_{\text{o1}}U^2}k\delta_{\text{cl}} - \Psi_{\text{p}} - c\hat{\Phi}_{\text{c}} + c\Phi_{\text{p}}\right), \tag{16a}$$

$$\hat{\Phi}_{\text{c}} = z + B^2 c\Psi_{\text{p}}, \tag{16b}$$

where $\hat{\Phi}_{\text{c}}$ is the estimated non-dimensional compressor mass flow rate, $\hat{\Psi}_{\text{c,ss}}$ is the non-dimensional steady-state compressor pressure rise at $\hat{\Phi}_{\text{c}}$, and $c = 5$ is the observer constant. The equations for $\dot{\Psi}_{\text{th}}$ and $\dot{\Phi}_{\text{p}}$ are the same as in Eq (9). It was demonstrated in [17] that the error between the estimated and actual mass flow value approaches zero for $c \geq 2(\partial\hat{\Psi}_{\text{c,ss}}/\partial\hat{\Phi}_{\text{c}}$. The observer constant c was selected considering the trade-off between the observer convergence rate and the propagation of the input sensor noise.

V. Experimental Results

The surge controller is implemented on the compressor test rig described in Section II, and the control test is performed at 16,290 rpm. The compressor was slowly driven into the surge region by closing the throttle valve and restricting the flow rate through the system. The waterfall plots in Figs. 8 and 9 show the frequency responses of the plenum pressure signals, measured at a range of the throttle valve openings. The results for the compressor without the surge controller is summarized in Fig. 8. The surge instability is observable as large peaks in the frequency response, located near 7 Hz and 21 Hz, in agreement with the frequencies of the unstable surge modes. At the current speed, surge is initiated at 17.7% throttle valve opening, and the frequency of the initial surge oscillation is near 21 Hz. This frequency corresponds to the acoustic resonance of the piping. If the flow is further restricted beyond the surge initiation point, the surge oscillation evolves to the full limit cycle. The frequency of the evolved surge instability is lowered to 7 Hz, and the amplitude of the surge component becomes nearly five times larger.

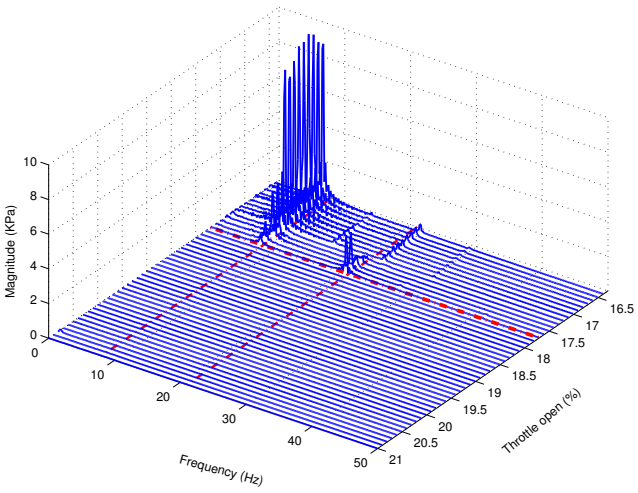

Fig. 8. Waterfall plot showing the frequency response of the measured plenum pressure signal as the compressor is driven into the surge region by closing the throttle valve and with the surge controller unactivated.

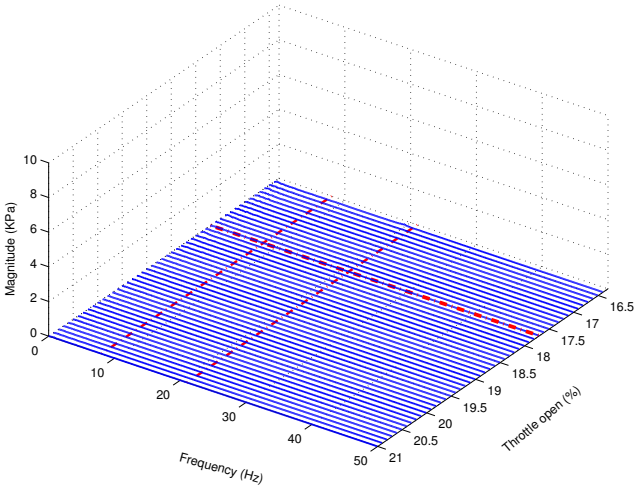

Fig. 9. Waterfall plot showing the frequency response of the measured plenum pressure signal as the compressor is driven into the surge region by closing the throttle valve and with the surge controller activated.

The measured frequency responses of the plenum pressure for the controlled compressor are presented in Fig. 9. When we compare the results in Fig. 9 to the observations corresponding to the uncontrolled compressor in Fig. 8, it is clear that the unstable modes of surge are stabilized by the surge controller. The large peaks near the frequencies of the unstable modes are no longer present in the controlled case, and the waterfall plot is flat for the range of valve openings that is presented in the figure. The compression system is able to maintain stability beyond the surge limit that was previously identified in Fig. 8, down to valve opening values as low as 16.4%.

The measured characteristic curves of the compression system before surge are shown in Fig. 10 with the surge controller activated and unactivated. The steady state compressor operating points with the surge controller unactivated are shown with the '$\circ$' markers in the figure. As expected, the compressor is stable in the high flow rate region, and the surge instability is initiated slightly to the left of the

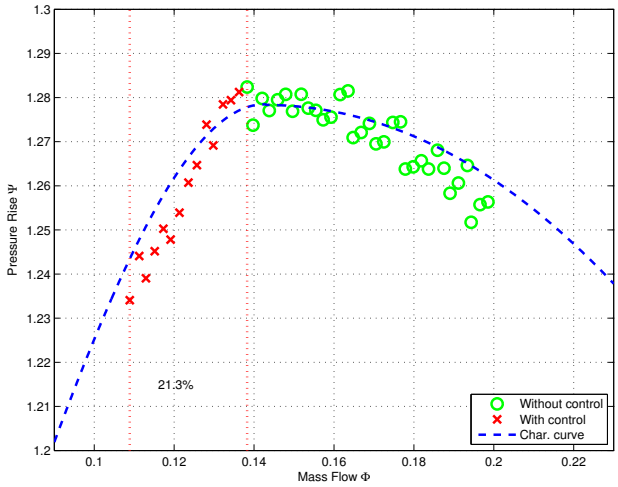

Fig. 10. Compressor steady state operation on the characteristic curve at 16,290 rpm with the surge controller activated and unactivated, respectively.

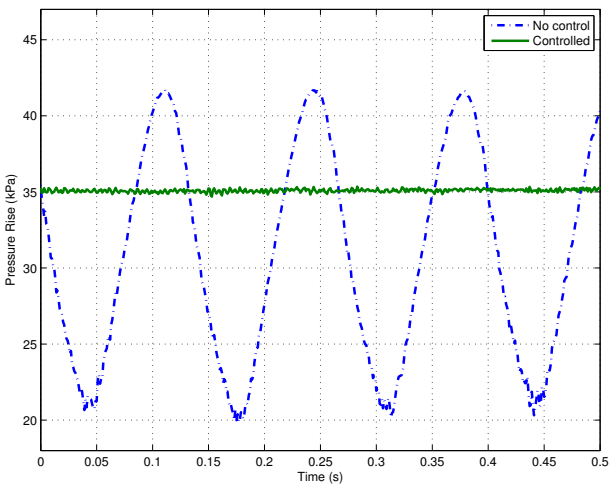

Fig. 11. Comparison of the measured plenum pressure rise signal at 16,290 rpm and 16.4% throttle valve opening for the compressor operating with the surge controller activated and unactivated, respectively.

peak pressure point. On the other hand, the '×' markers in the figure show measured operating points for the controlled compressor, and it is clearly observed that the system is stabilized for flow rates well inside the surge region. In fact, the flow rate can be reduced up to 21.3% of the surge point observed in the uncontrolled case before the first sign of surge appears. This would allow the compressor to operate at the peak pressure output without the need of a surge margin that would limit the compressor performance.

The measurements of the plenum pressure rise for the cases with the active surge controller activated and unactivated are compared in Fig. 11 with the throttle valve opening at 16.4%. In the uncontrolled case, the compression system is in the surge condition, and the frequency of the limit cycle is 7.33 Hz. When the active surge controller is activated, the unstable modes of the compression system are stabilized and the compressor operates at the equilibrium point. The peak-to-peak amplitude of the surge limit cycle in the uncontrolled system is nearly 63% of the equilibrium pressure rise. On the other hand, no significant oscillations can be observed in the pressure signal for the actively stabilized system.

VI. Conclusions

The use of the thrust AMB in the control of surge in centrifugal compressors was discussed in this paper. Based on a revised model of the compression system with piping acoustics and variable impeller clearance, a surge controller was derived and the effectiveness of the controller was tested. Experimental observations in an industrial sized compressor show promising performance of the surge controller, being able to reject the flow disturbances related to the surge instability. The implemented surge controller was capable of extending the stable flow range by 21.3%.

References

[1] R. C. Pampreen, *Compressor Surge and Stall*. Vermont, USA: Concepts ETI, 1993.

[2] B. de Jager, "Rotating stall and surge control: A survey," *Proceedings of the 34th IEEE Conf. Decision and Control*, pp. 1857–1862, 1995.

[3] A. H. Epstein, E. F. Williams, and E. M. Greitzer, "Active suppression of aerodynamic instabilities in turbomachinery," *Journal of Propulsion and Power*, vol. 5, pp. 204–211, Mar. 1989.

[4] J. S. Simon, L. Valavani, A. H. Epstein, and E. M. Greitzer, "Evaluation of approaches to active compressor surge stabilization," *ASME Journal of Turbomachinery*, vol. 115, pp. 57–67, Jan. 1993.

[5] G. L. Arnulfi, F. Blanchini, P. Giannattasio, and P. Pinamonti, "Extensive study on the control of centrifugal compressor surge," *Proceedings of the Institution of Mechanical Engineers, Part A: Journal of Power and Energy*, vol. 220, pp. 289–304, May 2006.

[6] J. T. Gravdahl and O. Egeland, "Centrifugal compressor surge and speed control," *IEEE Transactions on Control Systems Technology*, vol. 7, pp. 567–579, Sept. 1999.

[7] M. Krstić, D. Fontaine, P. V. Kokotović, and J. D. Paduano, "Useful nonlinearities and global stabilization of bifurcations in a model of jet enginer surge and stall," *IEEE Transactions on Automatic Control*, vol. 43, pp. 1739–1745, Dec. 1998.

[8] S. Y. Yoon, Z. Lin, K. T. Lim, C. Goyne, and P. E. Allaire, "Model validation for an amb-based compressor surge control test rig," *Proc. IEEE Conference on Decision and Controls*, pp. 756-761, 2009.

[9] S. Y. Yoon, Z. Lin, K. T. Lim, C. Goyne, and P. E. Allaire, "Control of compressor surge with active magnetic bearings," *Proc. IEEE Conference on Decision and Controls*, pp. 4323-4328, 2010.

[10] D. Sanadgol, *Active Control of Surge in Centrifugal Compressors Using Magnetic Thrust Bearing Actuation*. PhD thesis, University of Virginia, 2006.

[11] S. Y. Yoon, Z. Lin, C. Goyne, and P. E. Allaire, "An enhanced greitzer compressor model including pipeline dynamics and surge," *ASME Journal of Vibration and Acoustics*, vol. 133, p. 051005, 2011.

[12] S. Y. Yoon, Z. Lin, K. T. Lim, C. Goyne, and P. E. Allaire, "Model validation for an amb-based compressor surge control test rig," *ASME Journal of Vibration and Acoustics*, vol. 132, p. 061005, 2010.

[13] S. Y. Yoon, Z. Lin, C. Goyne, and P. E. Allaire, "An enhanced greitzer compressor model including pipeline dynamics and surge," *Proc. IEEE American Control Conference*, pp. 4446-4451, 2011.

[14] E. M. Greitzer, "Surge and rotating stall in axial flow compressors, part i, ii," *ASME Journal of Engineering for Power*, vol. 120, pp. 190–217, 1976.

[15] F. K. Moore and E. M. Greitzer, "A theory of post-stall transients in axial compressor systems: part i–development of equations," *ASME Journal of Engineering for Gas Turbines and Power*, vol. 108, pp. 68–76, Jan. 1986.

[16] W. C. Yang and W. E. Tobler, "Dissipative modal approximation of fluid transmission lines using linear friction model," *ASME Journal of Dynamic Systems, Measurements, and Control*, vol. 113, pp. 152–162, 1991.

[17] B. Bøhagen and J. T. Gravdahl, "On active surge control of compressors using a mass flow observer," *Proceedings of the 41st IEEE Conference on Decision and Control*, pp. 3684–3689, Dec. 2002.